Effect of the Tempering Heat Treatment on the Cu-Based Shape Memory Alloy Exposed to a Commonly used Corrosive Medium

Daniel Flores-Sanchez[1*], Miguel Ángel Suárez-Rosales[1], Midori Landa-Castro[1], Mirella Gutiérrez-Arzaluz[2], Manuel Palomar-Pardavé[1], Mario Romero-Romo[1*]

[1]Universidad Autónoma Metropolitana, Azcapotzalco. Área de Ciencia de Materiales, Área Ingeniería de Materiales. Departamento de Materiales. Av San Pablo No. 420, Col. Nueva el Rosario, Alcaldía Azcapotzalco, 02128 Ciudad de México.
[2]Universidad Autónoma Metropolitana, Azcapotzalco. Área de Química Aplicada, Departamento de Ciencias Básicas. Av San Pablo No. 420, Col. Nueva el Rosario, Alcaldía Azcapotzalco, 02128 Ciudad de México.

*Corresponding author: Daniel Flores-Sanchez, email: fs.daniel04@gmail.com; Mario Romero-Romo, email: mmrr@azc.uam.mx

Dedicated to Dra. Elsa Miriam Arce Estrada and Dr. Ignacio González Martínez who have been awarded Emeritus National Researchers in Electrochemistry by SNI-CONACYT system.

Abstract. In the present work, the corrosion behavior of the as-cast Cu-9Al-3Ag alloy, with shape memory, SMA, and with tempering heat treatments at two temperatures, 400 and 600 °C, were studied. These treatments were selected due to the austenite-martensite phase transition or vice versa. For this investigation, a 0.5 M NaCl electrolyte was used. Micrographs using optical microscopy and scanning electron microscopy show the martensite phase in the Cu-9Al-3Ag alloy, likewise, in the tempered samples the austenite-martensite phases were also observed. For the evaluation of the corrosion behavior, the Tafel model was implemented, for whose curves a potential of ±200 mV was used from the E_{corr}. It was observed that the sample with SMA presented a good resistance to corrosion, as well as the tempered samples, unlike the as-cast sample. Finally, impedance tests were carried out using a frequency range of 100 kHz to 10 mHz and an amplitude of 10 mV, in order to observe the resistances to the solution and to the charge transfer present in each one of the samples used.
Keywords: Corrosion; heat treatment; Tafel curves; EIS; shape memory alloy.

Resumen. En el presente trabajo se estudió el comportamiento de corrosión en la aleación Cu-9Al-3Ag en estado de colada, con memoria de forma en conjunto con tratamientos térmicos de revenido a temperaturas de 400 y 600 °C. Dichos tratamientos fueron seleccionados debido al cambio de transición de fase austenita-martensita o viceversa. Para esta investigación se utilizó un electrolito a 0.5 M NaCl. Las micrografías mediante microscopia óptica y microscopia electrónica de barrido muestran la fase martensita en la aleación Cu-9Al-3Ag, así mismo, en las muestras revenidas se puede observar las fases austenita-martensita. Para la evaluación del comportamiento de corrosión se implementaron las curvas de Tafel, en las cuales se utilizó un potencial de ±200 mV a partir del E_{corr}. Se observó que la muestra con SMA presento una buena resistencia a la corrosión al igual que las muestras revenidas a diferencia de la muestra en estado de colada. Por último, se realizaron pruebas de impedancia utilizando un rango de frecuencia de 100 kHz a 10 mHz y una amplitud de 10 mV, con la finalidad de observar las resistencias a la solución y a la transferencia de carga presentes en cada una de las muestras utilizadas.
Palabras clave: Corrosión; tratamiento térmico; curvas de Tafel; impedancia; memoria de forma.

Introduction

Shape memory alloys (SMA) or more generally materials have a singular response to heating, where after that features a return to the original shape after being initially deformed. Historically, one of the ever-present SMA is the material termed nitinol, a Ni-Ti alloy, which presents super plasticity effects, high ductility and excellent corrosion resistance [1]. Other groups of alloys such as Fe-based and Cu-based alloys also present the SMA characteristic, whereby being relatively newcomers, they have attracted attention to discover further different applications [2].

Within the Cu-base group, the Cu-Zn-Al and Cu-Al-Ni [3] alloys stand out, because they display some group peculiarities, such as: good physical properties, high thermal and electrical conductivity, as well as good resistance to corrosion. A focus on the manufacture of the Cu-Al alloy began due to the uniqueness of SMA, having as main reference the composition and heat treatment applied [4]. Said composition must be established between 8 and 11% of Al [5,6], while heat treating must be carried out until obtaining the β equilibrium phase, to perform later a rapid cooling to transform into the diffusion-less martensite phase [7]. The latter is considered very important because if the cooling is not fast enough, the decomposition of β to (α + γ_1) will result, which would imply the formation of pearlite instead of martensite [8], with the former being a constituent exhibiting lesser hardness.

For a material to be considered SMA, it suffices to display only one cycle between the austenite and martensite phases when subjected to temperature changes. Now, this was not the case in this paper, though the experiments with the Ag-containing ternary Cu-base alloys, have been nearly completed and there will be a paper comprising these findings. For the said cycle, the four temperatures that must be present are: the temperature at which austenite begins A_s and the temperature at which the martensite forms A_f austenite. On the other hand, when cooling is carried out, the temperature at which M_s martensite begins to form is considered, and finally, the temperature at which there is only M_f martensite [9,10].

The development of alloys with SMA is mainly influenced by the grain size, microstructure, texture and orientation [11,12], which has allowed the manufacture of materials emerging from various sectors of the industry such as medical implants, electrical connectors, fiber optic sensors, antennas for mobile phones, as well as anti-corrosion protective layers [13,14]. However, the investigations involving the Cu-Al alloy system have been poorly documented regarding the behavior of SMA in saline environments. This implies that the field of interest extends principally to marine, although aerospace applications have turned wide users, or those where a high resistance to corrosion is required. For this reason, various investigations have focused on adding a third alloying element such as Mn, Ni, Be or Ag [15,16] that chiefly allow stabilizing the β phase increasing, however, the fraction of martensite at room temperature.

Considering the above, this work focuses on showing the behavior of the alloy when exposed to a corrosive medium, such as NaCl, considering the addition of silver as a third element in the binary Cu-Al alloy, the which, according to the composition, displays the characteristic of having shape memory. Likewise, it seeks to analyze the effect that it has mainly on the transition temperatures of the austenite-martensite phase, for which tempering heat treatments have been applied at temperatures of 400 and 600 °C.

Experimental

Heat Treatments

The heat treatments were applied to three samples received in the cast state and were carried out in a Thermos Scientific Thermolyne model muffle at a temperature of 900 °C for a period of 120 minutes. After, the samples were quenched using water at room temperature as a cooling medium. Subsequently, the tempering treatment was carried out on two of the three samples using temperatures of 400 and 600 °C for each sample, for a period of 120 minutes. Likewise, water at room temperature was used again as a cooling medium. As with the case of NaCl, considering the addition of silver as a third element in the Cu-Al binary alloy, presents the characteristic of having shape memory. Similarly, this work seeks to analyze the effect that it has mainly on the

transition temperatures of the austenite-martensite phase, for which tempering heat treatments have been applied at temperatures of 400 and 600 °C.

Metallography

Conventional metallography surface preparation was used for the four samples, grinding them first over SiC (Buehler) in the grit range: 80 up to 1200. Polishing followed by means of a polisher (Buehler, EcoMet 30), MicroCloth® PSA cloth, and 0.3 µm alumina (Buehler, MicroPolishTM II), using a disk rotation of 250 rpm, concluding once a mirror finish was attained in each one of the samples. Finally, to reveal the microstructures, a reagent consisting of 150 ml ethyl alcohol (Sigma-Aldrich, 95 %), 25 ml HCl (Baker ACS, 36.5 – 38 %), and 10 g $FeCl_3$ (Sigma-Aldrich, 97 %).

Electrochemical experiments

Prior to running electrochemical experiments, the samples were immersed for about 15 minutes in the electrolyte. For the measurement of the Tafel curves, as well as for the impedance tests, the Solartron Modulab XM-MTS equipment was used together with a conventional three-electrode glass cell and 0.5 M NaCl as electrolyte solution. The electrodes consisted of Ag/AgCl, 3 M KCl (Sigma-Aldrich) as reference electrode, a graphite rod as counter electrode with a larger area than the working electrode, and as working electrodes the 4 samples used with a surface area of 1.5 cm^2. For the polarization curves, a potential of ± 200 mV (vs Ag/AgCl) was used with respect to the open circuit potential (OCP) obtained in each sample and 10 mVs^{-1} as potential scan rate. Finally, the impedance tests were performed using a frequency range of 100 kHz to 10 mHz, an amplitude of 10 mV, and 10 points per decade.

Microstructural examination

The microstructures of the worked samples were studied at low magnifications by optical microscopy (OM) using the Zeiss Axio Vert metallographic microscope. Likewise, they were also examined by scanning electron microscopy (SEM), by means of a ZEISS Supra 55VP equipment in the secondary electron imaging mode, coupled with an Energy Dispersive X-ray (EDX) detector.

Results and discussion

Microstructure

Fig. 1 shows the microstructure of the Cu-9Al-3Ag alloy in the as-cast state. Fig. 1**(a)** exhibits a microstructure reveals the grossest Cu-rich α phase grains that was the first constituent to be formed, hence, also it depletes the neighboring regions of aluminum with dendritic morphology resulting after solidification; the light-looking crystals represent the grains corresponding to the copper-rich α phase [17], while the dark interdendritic phase is related to a matrix containing CuAl, belonging to the β phase. Note that this is a rather coarse set of microstructural constituents, mostly present in elongated crystals. Likewise, due to slow cooling, which is not quite the case, the pro-eutectoid phase (α + γ₁) may appear [18]. It is observed that the dendritic grains present an elongated and uniformly distributed morphology. On the other hand, Fig. 1**(b)** represents a closer view of the the CuAl matrix by means of SEM. In this case, the CuAl matrix, belonging to the β phase, displays with greater detail a certain degree of roughness. There is formation of acicular structures although they do not pervade through the area, which may be indicative of a mixture of α + β phases.
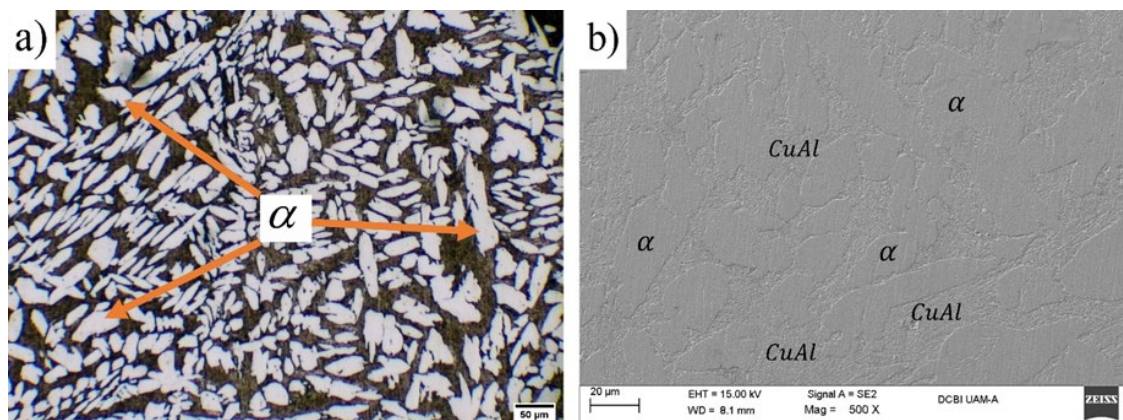
Fig. 1. Microstructure of the as-cast alloy sample, **(a)** at 25x by means of OM and **(b)** using SEM.

Further, Fig 2 **(a)** and **(b)** show the martensitic morphology that results from quenching, the amount of martensite was estimated from the Cu-Al phase diagram with the wt% data provided by EDX spectra recorded at 900 °C, this was 80%. Both micrographs reveal the formation of grain boundaries, which limit equiaxed grains within which the needles proper of the martensitic structures [19] appear to predominate the area under observation. According to Alaneme et al. [20], depending on the aluminum content, two types of martensitic transformation can occur, 6 M when the Al content is greater than 16 wt% and 2M when the content is lower. In this case, since the Al content is 9 wt%, the type of martensite corresponds to the 2M transformation with structure Face Centered Cubic (FCC).
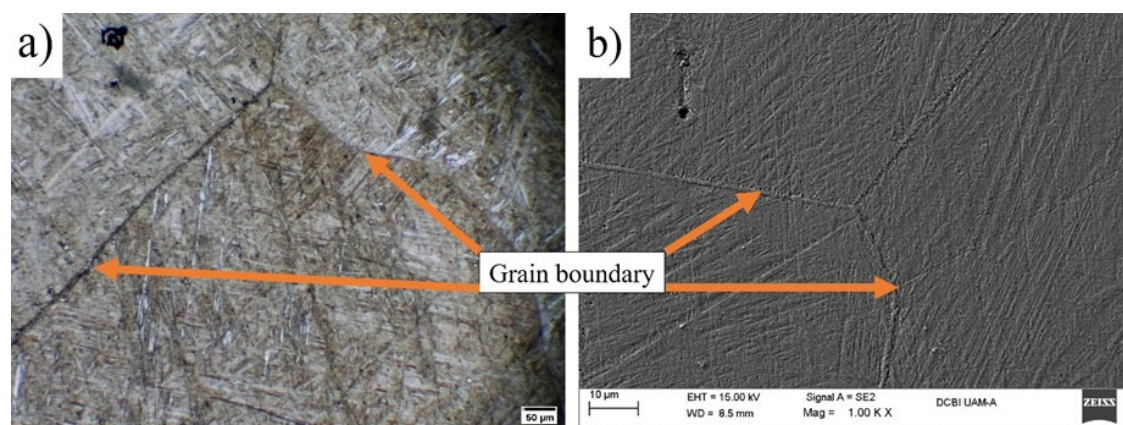
Fig. 2. Microstructure of the SAM alloy of Cu-Al, **(a)** observed at 25x by means of OM and **(b)** through SEM.

In order to be able to determine the morphologies present in the Cu-9Al-3Ag alloy after having obtained the martensitic structure, a tempering treatment was applied at working temperatures of 400 and 600 °C. Fig. 3**(a)** shows some clearer grain boundaries, unlike those presented in Fig. 2**(a)**. Likewise, the appearance of small globules is shown, which could be an indication of the coexistence of the α + β phases, which is in accordance with the composition of the EDX analysis and the Cu-Al [21] diagram, the predominant phase is α. On the other hand, Fig. 3**(b)** portrays the appearance of small Ag-rich precipitates [22] highlighted as light-colored globules.

Chemical composition (wt%)		
Cu	Al	Ag
59.99	4.06	35.95
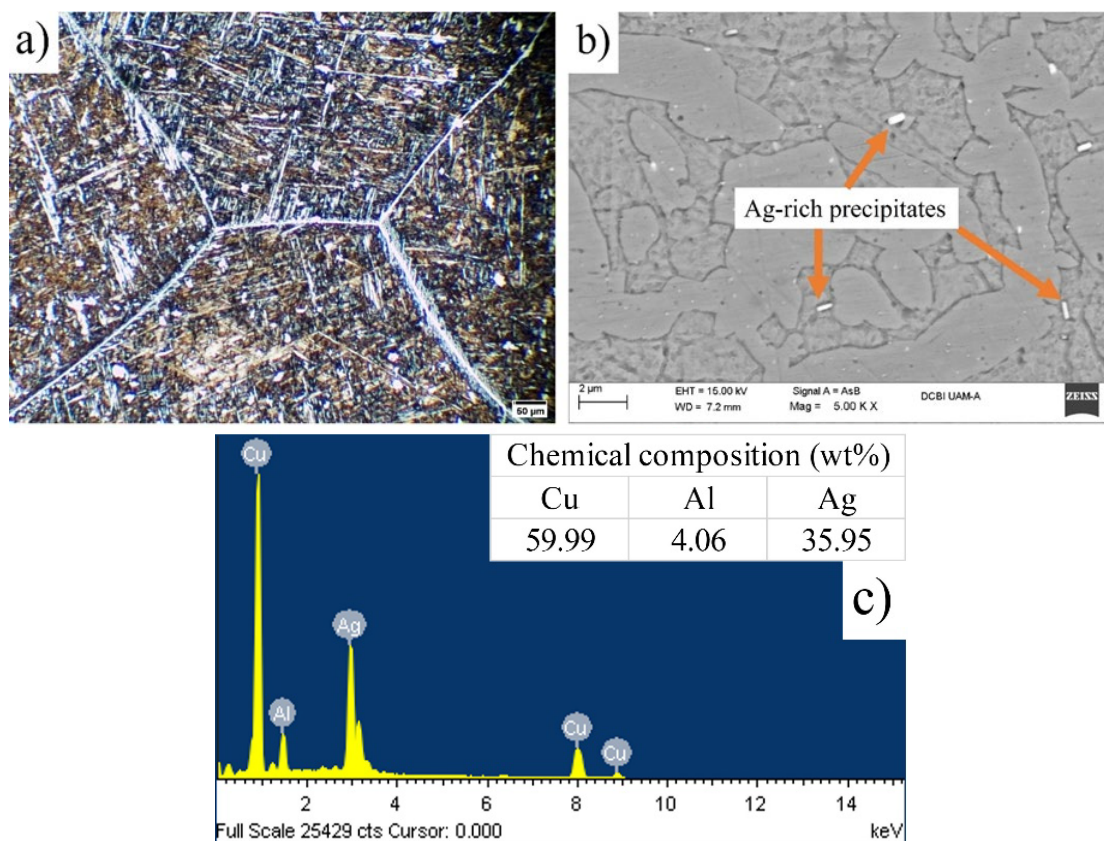
Fig. 3. Microstructure of the quenched and tempered sample at 400 °C, **(a)** observed at 25x through OM **(b)** by SEM and **(c)** EDX was recorded on over an silver particle.

The quenching and tempering heat treatments show clearly that the whitish silver precipitates have elongated slightly at random places of the microstructure. After the treatment at about 400 °C, Fig 3**(b)**, the silver globules appear to be more homogeneous in size, dispersing themselves mostly in the intergranular regions. To corroborate the compositions of the silver particles Fig. 3**(c)**, presents the EDX spectrum taken over selected silver particles such that this suggests segregation of the metal in diverse-shaped fragments.

Unlike Fig. 3, when the sample with SMA is tempered at a temperature of 600 °C, Fig. 4, it can be seen that the α phase begins to cover more area while the martensite begins to decrease. This can be verified in Fig. 4**(b)**, where the formation of elongated grains can be seen overlapping some traces of martensite [23]. Likewise, it is evident that the appearance of Ag-rich precipitates identified as white dots, are distributed homogeneously mainly over the grain boundaries. The voids mentioned that now appear solely in Fig 4**(b)** used to be occupied by small silver globules interspersed among the grains structure, that resulted from segregation after quench and tempering heat treatments at 600 °C.
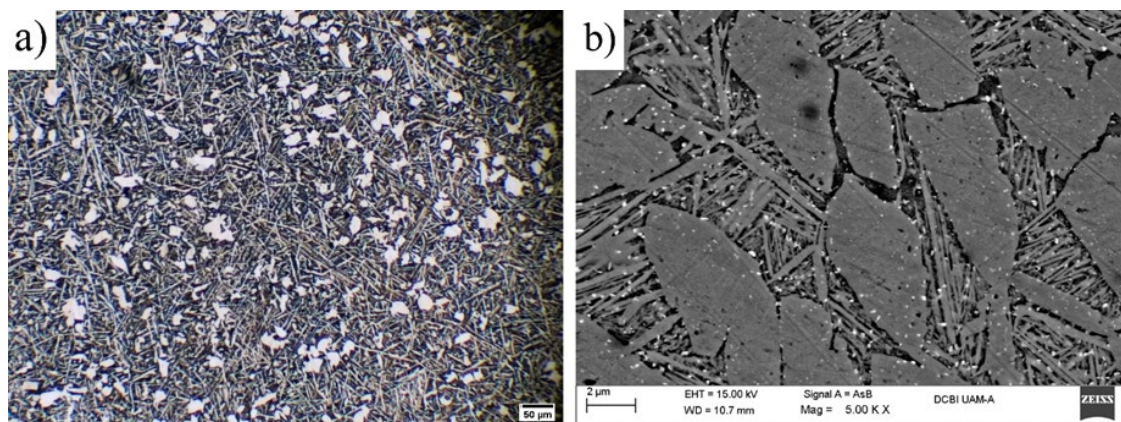
Fig. 4. Microstructure of the sample tempered a 600 °C, **(a)** OM micrograph taken at 25x and **(b)** by means of SEM.

Fig. 5 shows the EDX analyzes performed on each of the treated samples. Fig. 5**(a)** – 5**(d)** were taken over the entire SEM images. It is notable how the composition changes slightly with respect to the heat treatments applied, especially what concerns to Ag. As mentioned above, the addition of alloying elements to binary systems will provide substantial benefits [24] that will be reflected in some of the properties, whether physical, mechanical, among others. For this reason, Adorno et al. [25], investigated the effect of Ag on Cu-Al alloys, determining that Ag changes the characteristics of the martensitic transformation, stabilizing it at room temperature. Additionally, there is formation of Ag-rich phases.
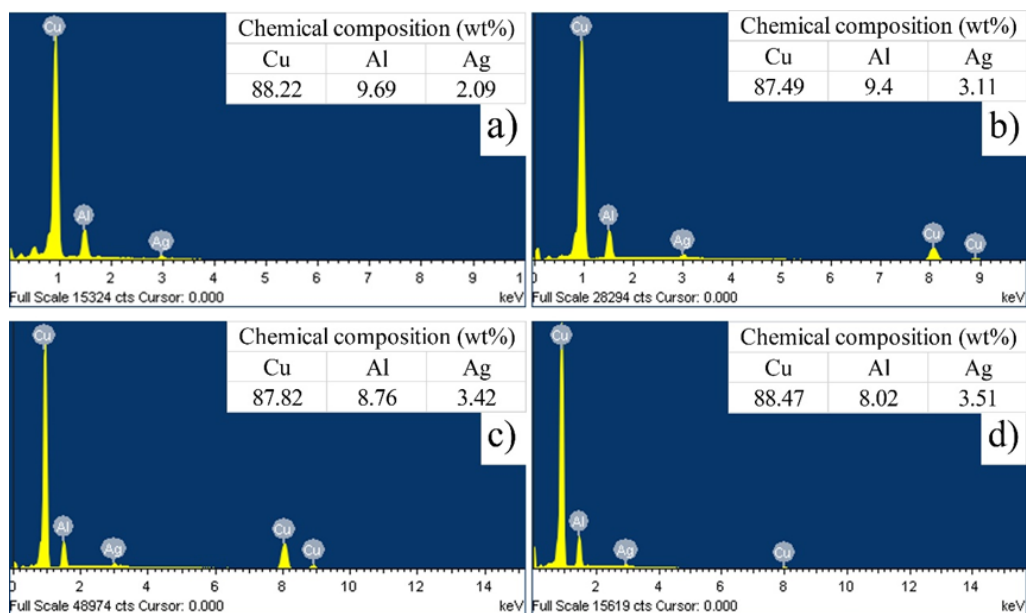
Fig. 5. EDX analysis of a samples **(a)** As-cast, **(b)** SMA, **(c)** Tempering 400 °C and **(d)** Tempering 600 °C.

Polarization curves

Fig. 6 shows the polarization behavior of the samples worked, with and without heat treatment. It is observed that the potentials (see Table 1) of the samples tempered at 400 and 600 °C are very likely and negative, unlike those obtained in the as-cast sample and with SMA in which positive potentials were obtained. Likewise, it is evident that the cathodic branches for all the samples are in very similar ranges while the anodic slopes vary significantly; this could be due to an irreversible dissolution of the material associated to a change in roughness of the present surface. On the other hand, the current densities for all materials present significant changes.
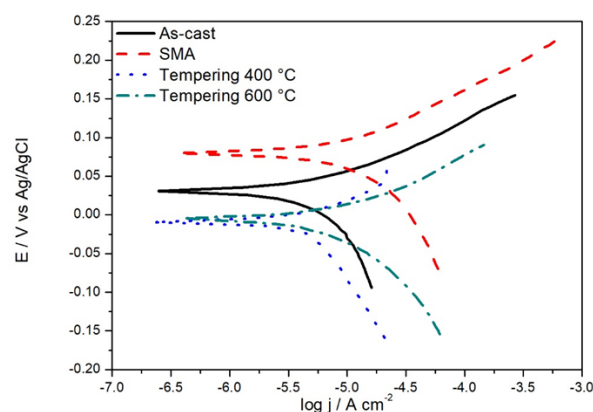
Fig. 6. Tafel plots, recorded at a potential of ± 200 mV from E_{corr} for each of the samples treated.

Table 1. Anodic β_a and cathodic β_c slopes of the Tafel plots done.

Samples	β_a (mV/dec)	β_c (mV/dec)	E_{corr} (mV)	j_{corr} (µA/cm^2)
As-cast	80	-332	29.2	7.1
SMA	86	-190	81	13.1
Tempering 600 °C	82	-179	-4	10.4
Tempering 400 °C	75	-228	-7.7	4.6

Table 1 shows that the SMA sample exhibits the largest corrosion potential, E_{corr}, and the greatest corrosion current density, j_{corr}. But after tempering the sample at 600 °C, the corrosion potential diminishes down to negative values along with the magnitude of the current density. Whereas at 400 °C, the tempering treatment has quite a similar effect insofar as the E_{corr} diminishes significantly in conjunction with the, j_{corr}. In addition, it is observed that both anodic and cathodic Tafel slopes present values within the ranges reported for Cu-Al base alloys [4] in conjunction with a third alloying element such as Be [26], Mn, Zn and Zr [27].

Further, the alloy with shape memory developed the greatest E_{corr}, followed by the as-cast simple. Alike the tempering treatments at 600 and 400 °C these reduced their corrosion potential till reaching negative values that strongly suggests a common behavior to ternary alloys that bear the presence of a relatively compact, outer layer capable of providing good continuity of coverage, notable compactness and substrate-adherence that seem competitive with other thicker aluminum-containing surface oxide/hydroxide films [28]. The silver particles that may be distributed over the surface altering the high embossment insufficiently to rupture the covering alumina surface blanket. Tempering at 400 °C is assumed to be the beneficial treatment.

Electrochemical impedance spectroscopy

Fig. 7 illustrates the electrochemical impedance results using Nyquist and Bode diagrams, parts a) and b) respectively, for each of the samples that were immersed in a 0.5 M NaCl solution. Likewise, in part a) the Electrical Equivalent Circuit (EEC) used to fit it to the data obtained is shown. The following elements stand out as part of the EEC: R_s, resistance of the NaCl solution; R_{ct}, resistance to charge transfer; Q, constant phase capacitance; W, Warburg [29,30].

From the Nyquist diagram it can be seen that the size of the semicircles is similar, except for the sample tempered at 400 °C, which presents the largest semicircle. This may be an indication that there is greater resistance to corrosion and may be attributed to a finer distribution of Ag in the alloy, including that of Ag-rich precipitates. However, when considering the Bode diagram, it is observed that the sample tempered at 400 °C has an angle greater than the previous one and close to 65°, indicating good corrosion resistance.
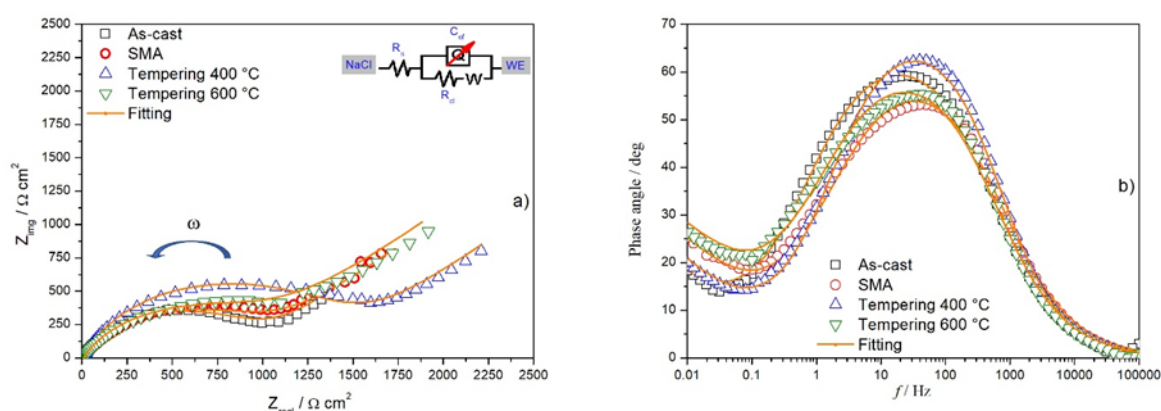
Fig. 7. Results of EIS of the alloy samples with and without heat treatment immersed in a 0.5 M NaCl solution at ambient temperature. **(a)** Nyquist and **(b)** Bode.

The results obtained from the circuit used are shown in Table 2, where an increase in R_{ct} for the heat-treated samples becomes apparent, which means that the phases present have a protective role in the alloy. On the other hand, the effective capacitance values, C_{ef}, are also indicated, which were calculated from the formula used by Sharma et al. [30], where it mentions that these values are associated with the Helmholtz equation and stipulates that the capacitance decreases due to the formation of a layer that reduces the corrosion area. This indicates that the sample treated at 400 °C, having the lowest C_{ef} and the highest R_{ct}, is the least predisposed to be corroded, which can be verified with the Tafel curves where the lowest corrosion current density was obtained.

Table 2. Parameters of the EEC used for the samples with and without heat treatment.

Samples	R_s	Q, Y_0	R_{ct}	n *	C_{ef}	Warburg, Y_0
	$\Omega \ cm^2$	$S \cdot sec^n$ $\times 10^{-5}$	Ω cm^2		$\mu F \ cm^{-2}$	$S \cdot sec^{0.5} \times 10^{-5}$
As-cast	5.9	36.8	971.9	0.7	236.8	746.1
SMA	12.1	19.7	1028	0.7	99.4	356.4
Tempering 600 °C	10	25.9	1052	0.7	148.4	285.8
Tempering 400 °C	11.4	11.2	1446	0.8	71.1	347

*Dimensionless constant phase element exponent.

Conclusions

This research focused on the effect of the quenching and tempering heat treatments on as-cast binary sample, to determine the behavior when exposed to a saline environment. As a result, a martensitic microstructure was obtained, which allows the alloy to display shape memory. On the other hand, the tempering treatments at 600 and 400 °C respectively, gave rise to notable morphology changes. It should be underlined that there was formation of fine silver particles that were evident at 400 °C and examined by means of EDX point analysis, corroborating the presence of elemental silver. From the Tafel curves, a decrease in the corrosion current density occurred together with the corrosion potential of the tempered sample indicating that the said temperature also meant diminishment of the corrosion process. This same effect was shown in the electrochemical impedance tests where the resistance to charge transfer increased, having the maximum value in the sample treated at 400 °C, while the effective capacitance showed the minimum value at said temperature, indicating the formation of a layer on the sample that decreases the area of corrosion.

On the other hand, the Randles circuit used showed a good fit in all the samples, evidencing that the sample with the largest semicircle corresponds to the tempering at 400 °C. Additionally, the Bode plot shows that the phase angle is resistive at high frequencies because the angles are slightly higher than 0°. While at medium frequencies, approximately, the tempered sample reaches an angle close to 65°. As a general conclusion, it is determined that the optimal tempering temperature that can be applied to this alloy is 400 °C since, for the purposes of corrosion rates in saline media, such as NaCl, it is the one that provides the best results.

Acknowledgements

References

1. Vrsalovic, L.; Gudic, S.; Percic, N.; Gojic, M.; Ivanic, I.; Kozuh, S.; Nagode, A.; Kosec, B. *Appl. Surf. Sci. Adv.* **2023**, *13*, 100380. DOI: https://doi.org/10.1016/j.apsadv.2023.100380.
2. Zheng, S.; Chen, S.; Hong, S.; Su, Z.; Zhang, J.; Wang, L.; Wang, C.; Yang, S. *J. Sci.:Adv. Mater. Devices.* **2022**, *7*, 100448. DOI: https://doi.org/10.1016/j.jsamd.2022.100448.
3. ASM International., in: *Copper and Copper Alloys,* Davis, J. R., Ed., ASM International, Ohio, **2001**, 121.
4. Souza, J. S.; Martins, C. R.; Silva, L. S.; Silva, R. A. G. *Mater. Chem. Phys.* **2022**, *282*, 125945. DOI: https://doi.org/10.1016/j.matchemphys.2022.125945.
5. Francis, R., in: *The Corrosion of Copper and its Alloys. A Practical Guide for Engineers*, NACE International, Texas, **2010**, 10.
6. Ying Ci, W.; Hafiz Akhbar, M.; Abu Bakar, T. A. *Jurnal Mekanikal.* **2018**, *41*, 31-36.
7. Turan, N. *GU. J. Sci.* **2023**, *11*, 210-221.
8. Magdalena, A. G.; Adorno, A. T.; Carvalho, T. M.; Silva, R. A. G. *J. Therm. Anal. Calorim.* **2011**, *106*, 339-342. DOI: 10.1007/s10973-011-1432-x.

9. Gustmann, T.; Dos Santos, J. M.; Gargarella, P.; Kuhn, U.; Van Humbeec, J.; Pauly, S. *Shap. Mem. Superelasticity*. **2017**, *3*, 24-36. DOI: 10.1007/s40830-016-0088-6.

10. Mohammed Dawood, N.; Kadhim Abid Ali, A. R. *Key Eng. Mater.* **2022**, *911*, 96-102. DOI: *10.4028/p-3jm065.*

11. Gojic, M.; Vrsalovic, L.; Kozuh, S.; Kneissl, A.; Anzel, I.; Gudic, S.; Kosec, B.; Kliskic, M. *J. Alloys Compd*. **2011**, *509*, 9782-9790. DOI: 10.1016/j.jallcom.2011.07.107.

12. Holjevac Grguric, T.; Manasijevic, D.; Kozuh, S.; Ivanic, I.; Anzel, I.; Kosec, B.; Bizjak, M.; Govorcin Bajsic, E.; Balanovic, Lj.; Gojic, M. *J. Alloys Compd*. **2018**, *765*, 664-676. DOI: https://doi.org/10.1016/j.jallcom.2018.06.250.

13. Placinta, C.; Stanciu, S.; Panainte-Lehadus, M.; Mosnegutu, E.; Nedeff, F.; Nedeff, V.; Tomozei, C.; Petrescu, T-C.; Agop, M. *Materials.* **2023**, *16*, 1441. DOI: https://doi.org/10.3390/ma16041441.

14. Chen, S.; Chen, X.; Guo, L.; Zheng, S.; Chen, F.; Wang, C.; Yang, S. *Vacuum*. **2023**, *210*, 111824. DOI: https://doi.org/10.1016/j.vacuum.2023.111824.

15. Silva, R. A. G..; Machado, E. S.; Adorno, A. T.; Magdalena, A. G.; Carvalho, T. M. *J. Therm. Anal. Calorim*. **2012**, *109*, 927-931. DOI:10.1007/s10973-011-1815-z.

16. Adorno, A. T.; Silva, A. G. *J. Therm. Anal. Calorim*. **2005**, *79*, 445-449. DOI: https://doi.org/10.1007/s10973-005-0082-2.

17. Li, G.; Liu, J. H.; Wang, W. K.; Liu, R. P. *Chin. Phys. B.* **2010**, *19*, 096202. DOI: 10.1088/1674-1056/19/9/096202.

18. Nwaeju, C. C.; Edoziuno, F. O.; Adediran, A.A.; Tuaweri, T. J.; Saravana Kumar, M. *Results Eng*. **2021**, *12*, 100295. DOI: https://doi.org/10.1016/j.rineng.2021.100295.

19. Guilemany, J. M.; Fernandez, J.; Zhang, X. M.; *Mater. Sci. Eng., A.* **2006**, *438-440*, 726-729. DOI: https://doi.org/10.1016/j.msea.2006.02.089.

20. Alaneme, K. K.; Uchenna Anaele, J.; Okotete, E. A. *Sci. Afr.* **2021**, *12*, e00760. DOI: https://doi.org/10.1016/j.sciaf.2021.e00760.

21. ASM Handbook., in: *Alloy Phase Diagrams*, ASM International, USA, **1992**, 44.

22. Carvalho, T. M.; Adorno, A. T.; Magdalena, A. G.; Silva, R. A. G. *J. Therm. Anal. Calorim.* **2011**, *106*, 333-338. DOI: 10.1007/s10973-010-1210-1.

23. Adorno, A. T.; Silva, R. A. G. *J. Mater. Sci.* **2005**, *40*, 6217-6221 DOI: 10.1007/s10853-005-3151-9.

24. Mazzer, E. M.; da Silva, M. R.; Gargarella, P. *J. Mater. Res.* **2022**, *37*, 162-182. DOI:10.1557/s43578-021-00444-7.

25. Adorno, A. T.; Silva, R. A. G. *J. Therm. Anal. Calorim.* **2003**, *73*, 931-938. DOI: https://doi.org/10.1023/A:1025863404768.

26. Montecinos., S.; Simison, S. *Corros. Sci.* **2013**, *74*, 387-395. DOI: http://dx.doi.org/10.1016/j.corsci.2013.05.012.

27. Mo-yang, Y.; Zhou, L.; Zhu, X.; Yong, P.; Ya-ping, L.; Zi-yan, S. *Trans. Nonferrous Met. Soc. China.* **2021**, *31*, 1012-1022. DOI: https://10.1016/S1003-6326(21)65557-7.

28. Saud, S. N.; Hamzah, E.; Abubakar, T.; Bakhsheshi-Rad, H. R. *Mater. Corros.* **2015**, *66*, 527-534. DOI: https://10.1002/maco.201407658.

29. Hernández-Espejel, A.; Palomar-Pardavé, M.; Cabrera-Sierra, R.; Romero-Romo, M.; Ramírez-Silva, M. T.; Arce-Estrada, E. M. *J. Phys. Chem. B.* **2011**, *115*, 1833-1841 DOI: https://dx.doi.org/10.1021/jp106851b.

30. Sharma, R.; Ullas, A. V.; Ji1, G.; Prakash, R. *J. Solid State Electrochem*. **2022**, *26*, 2883-2892 DOI: https://doi.org/10.1007/s10008-022-05293-w.